Title

Longitudinal evaluation of left ventricular substrate metabolism, perfusion, and dysfunction in the spontaneously hypertensive rat model of hypertrophy using small-animal PET/CT imaging.

Journal

Journal of nuclear medicine : official publication, Society of Nuclear Medicine, 54(11)

ISSN

0161-5505

Authors

Hernandez, Andrew M
Huber, Jennifer S
Murphy, Stephanie T
et al.

Publication Date

2013-11-01

DOI

10.2967/jnumed.113.120105

Peer reviewed

Longitudinal Evaluation of Left Ventricular Substrate Metabolism, Perfusion and Dysfunction in the SHR model of Hypertrophy using microPET/CT Imaging

Andrew M. Hernandez[1,2], Stephanie T. Murphy[2], Mustafa Janabi[1], Jennifer S. Huber[1], Gengsheng L. Zeng[3], Kathleen M. Brennan[1], James P. O'Neil[1], Youngho Seo[2,4,5], Grant T. Gullberg[1,2,5]

[1]*Life Sciences Division, Lawrence Berkeley National Laboratory, Berkeley, CA,*
[2]*Department of Radiology and Biomedical Imaging, University of California, San Francisco, CA,*
[3]*Department of Radiology, University of Utah, Salt Lake City, UT,*
[4]*Department of Radiation Oncology, University of California, San Francisco, CA,*
[5]*UC Berkeley – UCSF Graduate Program in Bioengineering, Berkeley and San Francisco, CA,*

Word Count: 5826

Running title: Molecular Imaging of Cardiac Hypertrophy

Key Words: *spontaneously hypertensive rat, myocardial substrate metabolism, myocardial perfusion, [^{18}F]fluorodihydrorotenol,*

Author correspondence: Andrew Hernandez, Lawrence Berkeley National Laboratory, Life Science Division, Berkeley, CA 94720 E-mail: amhernandez@lbl.gov

ABSTRACT

Myocardial metabolic and perfusion imaging is a vital tool for understanding the physiological consequences of heart failure. We used PET imaging to examine the longitudinal kinetics of 2-deoxy-2-[^{18}F]fluoro-D-glucose (FDG) and 14(R,S)-[^{18}F]fluoro-6-thia-heptadecanoic acid (FTHA) as analogs of glucose and fatty acid (FA) to quantify metabolic substrate shifts using the spontaneously hypertensive rat (SHR) as a model of hypertension-induced left ventricular hypertrophy (LVH). Myocardial perfusion and LV function were also investigated using a newly developed radiotracer [^{18}F]fluorodihydrorotenol (FDHROL). **Methods:** Dynamic electrocardiogram (ECG)-gated microPET/CT studies were acquired in eight SHR and eight normotensive Wistar-Kyoto (WKY) rats over their life cycle of ~20 months. We determined the myocardial influx rate constant (K_i) for [^{18}F]FDG and [^{18}F]FTHA and the wash-in rate constant (K_1) for [^{18}F]FDHROL. The ECG-gated [^{18}F]FDHROL data were used to quantify LV ejection fraction (LVEF) and end-diastolic volume (EDV). Lastly, blood samples were drawn to independently measure plasma concentrations of glucose and free fatty acids (FFA). **Results:** K_i^{FDG} and K_i^{FTHA} were higher in the SHR than the WKY ($p < 3\times10^{-8}$ and 0.005, respectively) independent of age. A decrease in K_i^{FDG} with age was evident when both rat models were combined (p=0.034). The SHR exhibited higher K_1^{FDHROL} ($p < 5\times10^{-6}$) compared to the control with no age-dependent trends in either model. Glucose plasma concentrations were lower in the SHR relative to control ($p < 4\times10^{-10}$) with an age-dependent rise in levels for the WKY ($p < 3\times10^{-4}$). Lastly, the FFA levels were similar between rat models but an increase with age was

evident only in the SHR ($p < 4\times10^{-5}$). **Conclusion:** The SHR exhibited alterations in myocardial substrate utilization at 8 months of age characterized by increased glucose and FA utilizations. At 20 months, the SHR developed LVH measured by decreased LVEF and increased EDV while simultaneously sustaining higher glucose and similar FA utilizations (compared to those of WKY), indicative of impaired energy efficiency in the failing heart. The elevated K_1^{FDHROL} in the SHR may reflect elevated oxygen consumption and decreased capillary density in the hypertrophied heart. From our findings, it appears that metabolic changes precede mechanical changes in the progression of LVH.

INTRODUCTION

Heart failure (HF) is the inability of the heart to provide sufficient blood flow to meet the metabolic needs of the body. Left ventricular hypertrophy (LVH) is one cardiac dysfunction that can result in HF. Hypertension, characterized by an increase in arterial blood pressure, is a common cause of LVH. Under healthy conditions, β-oxidation of free fatty acids (FFAs) provides 60-80% of ATP in the heart (*1, 2*). However, in the case of cardiac hypertrophy the heart exhibits an impaired substrate metabolism, which contributes to contractile dysfunction and continuous LV remodeling distinctive of the HF state (*3*).

A variety of *in vivo* noninvasive techniques are used to evaluate metabolic phenotype changes that occur in response to cardiac stress such as cardiac hypertrophy and HF (*4-7*). Specifically, molecular imaging using PET with 14(R,S)-[^{18}F]fluoro-6-thia-heptadecanoic acid (FTHA) and 2-deoxy-2-

[^{18}F]fluoro-D-glucose (FDG) are used to estimate fatty acid (FA) and glucose kinetics of the myocardial muscle in both human and small animals (*4, 8, 9*). [^{18}F]FTHA was synthesized by Degrado *et al (9)* in 1991 and was demonstrated to transport into the myocardium, undergo initial steps of beta-oxidation and subsequently be trapped in the cell. Only a small fraction has been identified to incorporate into triglycerides, thus the rate of FTHA retention by the myocardium is believed to reflect beta-oxidation of the long-chain FA (*9*). Furthermore, 2D echocardiographic examinations and myocardial gating techniques are used to quantify LV function in both humans and small animals (*10-14*). These techniques help determine the development of LVH, evidenced by a decreased left ventricular ejection fraction (LVEF) and increased end diastolic volume (EDV). In addition, increased oxygen demands generated by the hypertrophied LV increase myocardial oxygen consumption in the failing heart (*11, 15, 16*).

In summary, *in vivo* noninvasive molecular imaging has become a powerful tool to monitor myocardial metabolism phenotype, blood flow and overall cardiac function. Thus, it is timely to develop technology to longitudinally evaluate the progression of HF in small animals that can be translated to the clinic for the early stage identification and management of patients with cardiac hypertrophy.

The purpose of this study was to noninvasively examine the longitudinal alterations in myocardial metabolic phenotypes, blood flow and function in the spontaneously hypertensive rat (SHR) and compare these alterations with Wistar-Kyoto (WKY) controls. Our group used microPET/CT to assess myocardial

metabolic phenotypes using [^{18}F]FTHA and [^{18}F]FDG in the SHR and WKY rat models. In addition, we measured the wash-in rate constant (K_1) and overall heart function using a newly developed perfusion imaging agent [^{18}F]fluorodihydrorotenol (FDHROL), an analog of the mitochondrial binding rotenone. We hypothesized that the hypertrophied myocardium of the SHR would exhibit an increased [^{18}F]FDG influx rate constant (K_i^{FDG}) and suppressed [^{18}F]FTHA influx rate constant (K_i^{FTHA}), with an age-dependent decrease in the influx rate constant (K_i) of both tracers in the normal and failing heart. Lastly, we hypothesized that the SHR would show an initially elevated and subsequent age-dependent decrease in wash-in rate constant of [^{18}F]FDHROL relative to control.

MATERIALS AND METHODS

Synthesis of [^{18}F]FDG, [^{18}F]FTHA and [^{18}F]FDHROL

[^{18}F]FDG was routinely synthesized in the University of California San Francisco radiochemistry laboratory using the TRACERlab MX synthesis module (GE Healthcare). [^{18}F]FTHA and [^{18}F]FDHROL were both synthesized at UCSF according to previously published methods (*33)* using a FxFN synthesis module (GE Healthcare).

Animal Study Design

All imaging studies were performed in accordance with Institutional Animal Care and Use Committee (IACUC) approved protocols from both UCSF and Lawrence Berkeley National Laboratory. Eight male SHRs and eight male WKY normotensive rats were purchased from Charles River Laboratories. Imaging

began at approximately 8 months of age and the rats were imaged throughout their life cycle at separate time points corresponding to 8-9, 13-14, 19-20 and 22-23 months of age. All animals were freely fed standard Purina rat chow and water. The animals were nocturnal and mostly ate at night. During each time point, every animal was imaged using all three radiotracers ([^{18}F]FDG, [^{18}F]FTHA and [^{18}F]FDHROL) on separate days and thus separate anesthetic periods. Before [^{18}F]FDG and [^{18}F]FTHA imaging, food was taken away the evening before the studies. In comparison, the animals were not fasted for the [^{18}F]FDHROL acquisitions. Approximately 1 ml of blood was drawn from the tail vein of each rat once for each time point immediately following either the [^{18}F]FDG or [^{18}F]FTHA study.

Animal Imaging Protocol

All *in vivo* imaging was performed using a microPET/CT scanner (Inveon^{TM} dedicated PET docked with CT in the multimodality platform, Inveon, Siemens Medical Solutions). Each rat was anesthetized with gas isoflurane at ~2% concentration and medical grade oxygen. Electrocardiogram (ECG) electrodes were attached to the two front limbs and left hind limb to acquire signals used for cardiac gating. Rats were positioned on the scanning bed with the heart centered in the field of view of the scanner. Each radiotracer was administered via tail vein injection as a 0.5-1.5 ml bolus with activities: 54.8±7.40 MBq, 50.7±8.14 MBq and 49.2±8.88 MBq for [^{18}F]FDG, [^{18}F]FTHA and [^{18}F]FDHROL, respectively. Image acquisition began at the time of injection. The microPET/CT system was used to acquire dynamic ECG-gated list mode PET data over 60 minutes. The

PET data was subdivided into 38 frames as follows: 12×5 s, 6×10 s, 4×30 s, 6×60 s and 10×300 s. After the PET acquisition was complete, a separate CT scan was acquired with 120 projections of continuous rotation to cover 220° with an x-ray tube operated at 80 kVp, 0.5 mA and 160 ms exposure time.

The two-dimensional ordered-subsets expectation maximization (2D-OSEM) algorithm provided by the manufacturer was used for PET reconstruction, resulting in 128×128×159 matrices with a corresponding voxel size of 0.776×0.776×0.796 mm^3. The CT image was reconstructed using a conebeam Feldkamp reconstruction algorithm (COBRA) supplied by Exxim Computing Corporation. The matrix size of the reconstructed CT images was 512×512×662 with a voxel size of 0.190×0.190×0.190 mm^3. Photon attenuation correction was achieved for PET reconstruction using the co-registered CT-based attenuation map. No scatter correction was applied in this study.

Substrate/Biochemical Analysis

Blood samples obtained after either [^{18}F]FTHA or [^{18}F]FDG scans were spun in an Eppendorf 5415D microcentrifuge for ten minutes at 10,000 rpm. The plasma was separated and immediately stored at -80°C. The samples were then sent to AntiLytics to measure the circulating plasma substrates. Glucose and free fatty acid concentrations were measured using a Roche Hitachi 717 Chemistry Analyzer. The calibration levels were 0-500 mg/dL and 0-1200 μmol/L for glucose and FFA measurements, respectively. All measurements had a standard deviation of ≤ 5% as determined by AntiLytics.

PET Image Analysis

All reconstructed PET images were first analyzed using the Acquisition Sinogram Processing (ASIPRO, Siemens Medical Solutions) software in order to identify the ECG gates that corresponded to the end diastolic phase of the cardiac cycle. The diastolic phase was used to both alleviate smearing due to cardiac motion and reduce crosstalk measured activity between tissue and blood. Once these gates were identified, a new dynamic series was formed by summing the counts in each identified diastolic gate. The new images were then uploaded into Inveon^{TM} Research Workplace version 3.0 (Siemens Molecular Solutions) for tracer kinetic analysis. Myocardial time-activity curves (TACs) were generated by manually drawing a volume of interest (VOI) throughout the myocardium, with care taken to avoid the myocardial border. [^{18}F]FTHA and [^{18}F]FDHROL images displayed substantial liver uptake in both rat models compared to the [^{18}F]FDG images (**Figure 1**). To minimize spillover of radioactivity from the liver to the heart, the entire apex and mid-cavity septal wall were not defined within the VOI for any [^{18}F]FTHA or [^{18}F]FDHROL images. Tissue VOIs were then selected by placing voxels in 10 consecutive mid-ventricle slices. Only slices containing myocardium in 360° were selected. To generate blood time-activity curves for each tracer, small regions of interest (10-20 mm^3) were placed within the LV blood pool with care taken to avoid the boundary of the myocardium and LV cavity. Overall the diastolic images allowed for clear definition of VOI myocardium and blood pool regions well within anatomical boundaries, alleviating the need for partial volume correction over continuous slices.

Determination of [^{18}F]FDG and [^{18}F]FTHA Influx Rate Constant

The myocardial influx rate constants from the PET dynamic data were estimated using the multiple-time Patlak graphical analysis approach (*4, 17*). The last 10 time frames (10-60 min) were used to determine K_i^{FDG} and K_i^{FTHA} via linear regression. Although the myocardial metabolic uptake rate conventionally can be calculated by using K_i, plasma concentration and the lumped constant, the lumped constant is not truly constant and varies with respect to preferential uptake of the tracer (*18*). Thus, for the scope of this study K_i^{FDG} and K_i^{FTHA} are reported.

Determination of Wash-in Rate Constant using [^{18}F]FDHROL

The myocardial wash-in rate constant of [^{18}F]FDHDROL was estimated using a single tissue compartment model, based on Kety's theory for an inert freely diffusible tracer that originates from Fick's law of diffusion (*19*). This model has the exchange of radiotracer between the whole blood compartment and a single tissue compartment measured by two rate constants, K_1 and k_2. K_1 is defined as the wash-in rate constant out of the LV blood pool into the extravascular and cellular spaces of the myocardium and k_2 is defined as the wash-out rate constant out of myocardium into the LV blood pool. A previously published closed-form algorithm was used to fit the [^{18}F]FDHROL TACs to this single tissue model (*20*). This algorithm alleviates the issues with convergence due to local minima when compared to classic nonlinear least-squares estimation.

Evaluation of Cardiac Function

The ECG-gated [^{18}F]FDHROL images were used to evaluate the left ventricular ejection fraction and end-diastolic volume. These two parameters were measured

using the clinical cardiac software Myovation designed for an Xeleris Workstation (GE Healthcare). The images were first scaled to the dimensions of a human heart for compatibility with the clinical software. The resulting images were reoriented into short axis, horizontal long axis and vertical long axis views for subsequent automatic segmentation using the Myovation segmentation algorithm. Visual assessment was used to ensure the segmentation was accurate and adjustments were made when necessary.

Statistical Analysis

All animal laboratory and imaging results are presented as mean ± standard deviation. Two-Way analysis of variance (ANOVA) was used to determine the main effect of contributions from each independent variable (*i.e.*, rat model or time) and was also used to identify the possibility of an interaction effect between the variables. For example, the main effect of the rat model is the difference between the means of the dependent variable (*e.g.*, myocardial influx constant) for the two rat models when time is ignored. Furthermore, a significant interaction effect between rat model and age exists if there are age-dependent differences in the change of the dependent variable (*e.g.,* wash-in rate constant) for each individual rat model. In addition, Welch's unpaired t-test was used to compare the mean of the two rat models with unequal variances at a given time point, in addition to the post mortem heart-to-body weight ratio. The use of Welch's unpaired t-test will be indicated explicitly. P values less than 0.05 were considered statistically significant for all tests.

RESULTS

Animal Characteristics

All eight spontaneously hypertensive rats developed hypertrophy and the eventual onset of HF with a life span of 20 ± 3 months. Ejection abnormalities associated with the development of hypertrophy were verified by an elevated EDV and subsequent drop of LVEF in the SHR compared to the control, as shown in **Figure 2**. In particular, the SHR demonstrated a significant age-dependent increase in EDV ($p < 9\times10^{-5}$) whereas the control stayed constant with age. Furthermore, a significant interaction in LVEF between model and age was manifested as an age-dependent decrease in the SHR and an age-dependent increase in the control ($p < 2\times10^{-6}$). Lastly, autopsy reports revealed that the heart-to-body weight ratio was 0.0068 ± 0.0012 for the SHRs and 0.0037 ± 0.0003 for the controls ($p < 0.0001$) indicative of a hypertrophied heart in the SHR model.

Plasma Circulation Measurements

Figure 3 is a plot of the mean circulating glucose and free fatty acid plasma concentrations over the lifetime of the animals. The SHR showed lower glucose levels relative to the control ($p < 4\times10^{-10}$). Moreover, a significant age-dependent increase in glucose plasma concentration was apparent in the control ($p < 1\times10^{-3}$) relative to the SHR. Although no significant difference was seen in FFA plasma concentrations between the two models ($p = 0.68$), a significant interaction between rat model and time was manifested as an age-dependent increase for the SHR ($p < 4\times10^{-5}$).

[^{18}F]FTHA Kinetics in Myocardial Tissue

Roughly 2 minutes after bolus injection of [^{18}F]FTHA, uptake in the heart was sufficient to provide clear distinction of myocardial borders. As mentioned above, substantial liver uptake was visible within both rat models as shown in **Figure 1B**. The TAC generated from each myocardial VOI displayed increased myocardial activity followed by a plateau after roughly 4 minutes. There was no visible decline in myocardial activity throughout the remainder of the scan implying significant trapping of [^{18}F]FTHA in the tissue. The whole blood TAC showed an early sharp spike in radioactivity and a subsequent plateau, indicative of the administered bolus injection followed by rapid washout from the blood. K_i^{FTHA} was determined using this image derived input function from whole blood and the corresponding myocardial TAC. For all rat models, the graphical analysis plots were linear indicating radiotracer trapping in the myocardium. **Figure 4b** shows the mean K_i^{FTHA} for each model at four separate time points. Contrary to our hypothesis, the SHR demonstrated significantly higher K_i^{FTHA} than the control, ignoring age (p = 0.005). This elevated K_i^{FTHA} in the SHR was however only evident at 8 months of age and no difference was seen after one year. Furthermore, no effect was seen with respect to age (p = 0.087) or the interaction of rat model and age (p = 0.515).

[^{18}F]FDG Kinetics in Myocardial Tissue

As expected, the fasted WKY showed little myocardial [^{18}F]FDG uptake. In comparison, the fasted SHR showed significant uptake of [^{18}F]FDG, providing excellent image quality and relatively no liver contamination, as seen in **Figure**

1C. **Figure 5** compares the TACs for [^{18}F]FDG uptake generated from both rat models. Myocardial TACs showed substantial uptake in the SHR relative to the WKY. The early peak seen in the myocardial TACs for both models is due to spillover from LV blood pool to tissue seen within the first two minutes of acquisition. Patlak graphical analysis plots were linear indicating trapping of radiotracer in the heart muscle. K_i^{FDG} in the SHR was higher than the control ($p < 3\times10^{-8}$) when all time points were combined, seen in **Figure 4a**. In addition, K_i^{FDG} decreased significantly with age when both models were pooled together ($p = 0.034$). These results support our hypothesis that the hypertrophied myocardium of the SHR will show an elevated K_i^{FDG} compared to control and an age-dependent decrease in both models.

[^{18}F]FDHROL Perfusion Evaluation

[^{18}F]FDHROL provided outstanding flow versus extraction characteristics, which allowed for clear separation of the LV blood pool and myocardium approximately 2 minutes after bolus injection. **Figure 6** is an example of the myocardial and whole blood TACs seen in a 14-month old SHR. The plot depicts quick uptake of the tracer in the myocardium and rapid extraction from the LV blood pool. **Figure 6** also shows the curve fit based on the closed form algorithm (*20*). Using this algorithm, the wash-in rate constant (K_1) was measured to be higher in the SHR relative to the control ($p < 5\times10^{-6}$), as shown in **Figure 7**, supporting our hypothesis. Contrary to our hypothesis, no significant effect was seen with age ($p = 0.058$) or the interaction of rat model and age ($p = 0.898$).

DISCUSSION

This study is the first of its kind to longitudinally monitor substrate shifts in myocardial fatty acid and glucose metabolism as well as perfusion with *in vivo* imaging during the progression of HF in a rat model of hypertension-related pathophysiology. Our results showed that in early stages of HF at eight months of age, both K_i^{FDG} and K_i^{FTHA} for the SHR model were greater compared to the control ($p < 2\times10^{-3}$ and $p < 1\times10^{-3}$, respectively using Welch's unpaired *t*-test). After roughly one year of age the failing heart began to utilize glucose as a metabolic fuel with no significant difference in K_i^{THA} between the two models. These radiotracer K_i differences are related to differences in circulating plasma substrates. At early time points there is no clear difference between rat models, but elevated plasma FFA concentrations and lower glucose levels relative to controls are evident in the SHR beginning at ~20 months. Furthermore, we found a higher wash-in rate constant of [^{18}F]FDHROL in the SHR model compared to control. The onset of ejection abnormalities, evidenced by suppression of LVEF, align with the aforementioned 20 months of age and further support the idea that the SHR develops hypertrophy after roughly one and a half years of age (*3*, *12*, *21*). This hypertrophy is evidenced by: reliance on glucose oxidation driven cardiac metabolism, elevated levels of circulating FFA plasma concentrations, low levels of glucose and an increase in blood flow to support increasing oxygen demands of the failing heart.

Fatty Acid Substrate Utilization

Our previous longitudinal study using dynamic microSPECT imaging of [^{123}I]BMIPP indicated a higher FA metabolic rate in two control rats compared with two SHR at 14 months and a general decrease with age in both models (*22*). The inconsistency between the FFA metabolism seen in our previous SPECT [^{123}I]BMIPP study and the present PET [^{18}F]FTHA study is likely due to the fact that the SHR rats in the [^{123}I]BMIPP study were not fasted. Hajri *et al.* also found that FA oxidation is reduced in the heart of the SHR by comparing the biodistribution of the slowly oxidized FA analog [^{125}I]BMIPP in WKY controls and SHR (*23*). The suppressed FA uptake in this spontaneous hypertensive rat model of HF is expected due to the deficiency of CD36, a membrane FA transporter, which impairs transport of long chain FAs across the cell membrane. These findings support the idea of a down-regulation of FA oxidation as LVH progresses (*3*).

Although the measurement of circulating FFA plasma concentrations showed no significant difference between models when time was ignored, an age-dependent increase in the SHR FFA levels relative to the control was seen. Thus, at 20 months of age the SHR had higher FFA levels relative to control ($p = 0.035$, as determined by Welch's unpaired t-test). The similarity in FFA levels between rat models at early ages is likely due inherent increased circulating FFA plasma concentrations in the fasting state for both models (*3*). The age-dependent increase in levels for the SHR combined with the aforementioned synchronous ejection abnormality further validates the findings that development of LVH and

eventual onset of HF is accompanied by an elevation in FFA plasma concentration.

Glucose Uptake and Substrate Metabolism

The preference of metabolic fuel in the failing heart has been investigated in order to understand the subtle changes in substrate shifts between FFAs and glucose (*4, 7, 21*). Consistent with our findings, Dodd *et al.* determined with hyperpolarized carbon-13 (^{13}C) *in vivo* imaging that by 15 weeks of age, the SHR experiences significant LVH and substrate metabolic transition away from FA β-oxidation driven cardiac metabolism to an increase in glucose oxidation (*21*). Additionally, we found increased K_i^{FDG} in the SHR at early ages, 8-9 months, which is consistent with the findings of Hajri et al (*23*) who found that at even earlier times (*i.e.*, 9-10 weeks) the SHR already showed increased myocardial glucose uptake. [^{18}F]FDG uptake by the heart also relies on the rate of delivery to the myocardium, which is directly related to circulating glucose plasma concentrations (*24*). The lower glucose plasma levels determined in this study for the fasted SHR is likely due to the rapid extraction of glucose from the capillary bed which is necessary to meet the energy demands of the failing heart. These findings are again consistent with those found by Hajri *et al.* using non-fasted SHRs indicating a lack of dependence on starvation, with circulating glucose levels.

[^{18}F]FDHROL Perfusion Imaging

[^{18}F]FDHROL proved to be an outstanding tracer for analyzing perfusion owing to its characteristics of excellent extraction versus flow. This radiotracer provided an exemplary marker of flow with improved contrast of myocardium to

background and thus improved precision and bias of estimated perfusion parameters**.** Myocardial blood flow in the spontaneously hypertensive model has been quantitatively assessed using several different modalities (*15, 16, 25*); however, none of these studies have longitudinally evaluated the changes of myocardial blood flow in the hypertrophic onset of HF. We found that K_1 was significantly higher in the SHR ($p < 5\times10^{-6}$) similar to results found previously (*15, 16*). The elevated K_1 in the SHR is likely due to increased needs of the hypertrophied myocytes. Enlarged muscle fibers inherently increase the diffusion distance of oxygen and make it a far less efficient process, thus requiring relatively more oxygen to meet the demands of the failing heart (*26*).

The Failing Heart

Overall there seems to be a discrepancy amongst investigations of myocardial metabolic phenotypes. HF is by no means a highly specific disease but is a complex system that is dependent on etiology, duration, endothelial dysfunction, and the simultaneous occurrence of complicating disorders such as diabetes, hypertension, obesity and genetics (*3*). All of these factors produce a large heterogeneity amongst the available patient and animal models that one can study. In addition to FA fueled myocardial metabolism, the heart utilizes endogenous substrates of glycogen and triglycerides as buffers for variations in diet and hemodynamics (*27*). Korvald *et al.* found that under stressed conditions the heart oxidizes the most efficient fuel, which depends on arterial substrate concentration, workload and oxygen supply (*28*). They found that the efficiency of glucose as a metabolic phenotype could exceed that of FAs by as much as 40%. In advanced

stages of HF there is a down regulation of FA oxidation, increased glycolysis and oxidation from the storage buffers, reduced respiratory chain activity and impaired reserve for mitochondrial oxidative flux (*3, 29*). Overall this prevents the heart from effectively transferring chemical energy from metabolism to contractile work. What is not understood is the time course and molecular mechanisms for this switch in substrate oxidation.

The SHR has been widely used as a model of the transition from compensated LV hypertrophy to systolic HF exhibiting alterations in myocardial metabolism, perfusion and overall cardiac function in the progression of HF (*12, 30, 31*). The drop in LVEF and increase in EDV for the SHR in this study distinguished the transition to systolic failure characterized by eccentric hypertrophy. As the heart could no longer adequately pump through the arteries, the increased venous pressure began to build up behind the failing heart. This elevated upstream capillary hydrostatic pressure eventually led to the discharge of fluid across the capillary endothelium producing edema in the lungs (*26*). All SHRs imaged in this experiment were found with fluid in their lungs upon post mortem biopsy and dilated cavity volumes were visually apparent, confirming the development of HF.

Study Limitations

The main limitations of this study are (1) small sample size, (2) regional myocardial [^{18}F]FTHA and [^{18}F]FDG uptake related to regional variations in blood flow and (3) limited physiological data (*i.e.,* no blood pressure, limited metabolite measurements). We began with eight SHR and eight WKY rats and

ended with one SHR and four WKY during the last time point at ~2 years. Thus, the value determined for any given parameter, at the last time point, is not at all representative of the entire cohort of SHR. Moreover, since there is a heterogeneity in the time course of transition from compensated LVH to failure in the SHR, the average at a given time point may not represent the same stages in the development of LVH and onset of HF. Further work will use a larger cohort of SHRs and will look at defining the time points such that the final imaging study lies before the majority of the SHRs have to be euthanized due to progressive HF symptoms. Irreversible experimental circumstances also limited the sample size at a given time point (*i.e.*, sample waking up and crawling out of the detector, inability to inject tracer in tail vein and significant sample motion in multiple frames most likely due to inadequate levels of anesthesia). Moreover, metabolite corrections require rapid blood sampling immediately following IV injection. Obtaining blood samples is a difficult task that can lead to serious blood depletion; however, the ability to correct for metabolites offers more accurate kinetic modeling. Future work will utilize previously developed microsampling techniques to minimize blood loss while still providing sufficient sampling for substrate levels and metabolite analysis (*32*). Lastly, the hypertrophied heart involves thickening of myocardium walls that cause global perfusion abnormalities leading to heterogeneous myocardial perfusion. Regional myocardial metabolism and perfusion analysis could offer the possibility of locating the regional defects associated with the transition from LVH to HF in the SHR.

CONCLUSION

Our study has developed techniques to measure alterations in glucose and fatty acid substrate utilization during the progression of HF, as well as correlated these changes with changes in perfusion and overall cardiac function. Longitudinal evaluation allowed for the study of the succession of events related to hypertrophy beginning from the pre-hypertrophic stage in the SHR. A significant elevation in the myocardial [^{18}F]FDG influx rate constant was evident in the 8-month old SHR before development of a hypertrophied heart (*i.e.*, no ejection abnormality). Thus it is likely that metabolic alterations precede mechanical alterations in the onset of LVH. This observation may help in the development of therapeutic approaches directed at preventing and managing LVH.

Acknowledgements

This study was support by the National Institutes of Health of the U.S. Department of Health and Human Services under grant R01-EB007219; and by the Director, Office of Science, Office of Biological and Environmental Research of the U.S. Department of Energy under contract DE-AC02-05CH11231. We also want to thank Rod Gullberg of Clearview Statistical Consulting for his assistance with the statistical analyses.

References:

1. Neely JR, Morgan HE. Relationship between carbohydrate and lipid metabolism and the energy balance of heart muscle. *Annual review of physiology.* 1974;36:413-459.

2. Bing RJ, Siegel A, Ungar I, Gilbert M. Metabolism of the human heart. II. Studies on fat, ketone and amino acid metabolism. *The American journal of medicine.* Apr 1954;16(4):504-515.

3. Stanley WC, Recchia FA, Lopaschuk GD. Myocardial substrate metabolism in the normal and failing heart. *Physiological reviews.* Jul 2005;85(3):1093-1129.

4. Taylor M, Wallhaus TR, Degrado TR, et al. An evaluation of myocardial fatty acid and glucose uptake using PET with [18F]fluoro-6-thia-heptadecanoic acid and [18F]FDG in Patients with Congestive Heart Failure. *Journal of nuclear medicine : official publication, Society of Nuclear Medicine.* Jan 2001;42(1):55-62.

5. de las Fuentes L, Herrero P, Peterson LR, Kelly DP, Gropler RJ, Davila-Roman VG. Myocardial fatty acid metabolism: independent predictor of left ventricular mass in hypertensive heart disease. *Hypertension.* Jan 2003;41(1):83-87.

6. Kudo T, Fukuchi K, Annala AJ, et al. Noninvasive measurement of myocardial activity concentrations and perfusion defect sizes in rats with a new small-animal positron emission tomograph. *Circulation.* Jul 2 2002;106(1):118-123.

7. Davila-Roman VG, Vedala G, Herrero P, et al. Altered myocardial fatty acid and glucose metabolism in idiopathic dilated cardiomyopathy. *Journal of the American College of Cardiology.* Jul 17 2002;40(2):271-277.

8. Maki MT, Haaparanta M, Nuutila P, et al. Free fatty acid uptake in the myocardium and skeletal muscle using fluorine-18-fluoro-6-thia-heptadecanoic acid. *Journal of nuclear medicine : official publication, Society of Nuclear Medicine.* Aug 1998;39(8):1320-1327.

9. DeGrado TR, Coenen HH, Stocklin G. 14(R,S)-[18F]fluoro-6-thia-heptadecanoic acid (FTHA): evaluation in mouse of a new probe of myocardial utilization of long chain fatty acids. *Journal of nuclear medicine : official publication, Society of Nuclear Medicine.* Oct 1991;32(10):1888-1896.

10. Szymanski MK, Kruizinga S, Tio RA, et al. Use of gated 13N-NH3 micro-PET to examine left ventricular function in rats. *Nuclear medicine and biology.* Jul 2012;39(5):724-729.

11. Katz AM. Mechanisms and abnormalities of contractility and relaxation in the failing heart. *Cardiologia.* Dec 1993;38(12 Suppl 1):39-43.

12. Bing OH, Brooks WW, Robinson KG, et al. The spontaneously hypertensive rat as a model of the transition from compensated left ventricular hypertrophy to failure. *Journal of molecular and cellular cardiology.* Jan 1995;27(1):383-396.

13. de las Fuentes L, Soto PF, Cupps BP, et al. Hypertensive left ventricular hypertrophy is associated with abnormal myocardial fatty acid metabolism and myocardial efficiency. *Journal of nuclear cardiology : official publication of the American Society of Nuclear Cardiology.* May-Jun 2006;13(3):369-377.

14. Porenta G, Kuhle W, Sinha S, et al. Parameter estimation of cardiac geometry by ECG-gated PET imaging: validation using magnetic resonance imaging and echocardiography. *Journal of nuclear medicine : official publication, Society of Nuclear Medicine.* Jun 1995;36(6):1123-1129.

15. Granstam SO, Granstam E, Fellstrom B, Lind L. Regional haemodynamic differences between normotensive and spontaneously hypertensive rats--a microsphere study. *Physiological research / Academia Scientiarum Bohemoslovaca.* 1998;47(1):9-15.

16. Nishiyama K, Nishiyama A, Frohlich ED. Regional blood flow in normotensive and spontaneously hypertensive rats. *The American journal of physiology.* Mar 1976;230(3):691-698.

17. Patlak CS, Blasberg RG, Fenstermacher JD. Graphical evaluation of blood-to-brain transfer constants from multiple-time uptake data. *Journal of cerebral blood flow and metabolism : official journal of the International Society of Cerebral Blood Flow and Metabolism.* Mar 1983;3(1):1-7.

18. Hashimoto K, Nishimura T, Imahashi KI, Yamaguchi H, Hori M, Kusuoka H. Lumped constant for deoxyglucose is decreased when myocardial glucose uptake is enhanced. *The American journal of physiology.* Jan 1999;276(1 Pt 2):H129-133.

19. Kety SS. The theory and applications of the exchange of inert gas at the lungs and tissues. *Pharmacological reviews.* Mar 1951;3(1):1-41.

20. Zeng GL, Hernandez A, Kadrmas DJ, Gullberg GT. Kinetic parameter estimation using a closed-form expression via integration by parts. *Physics in medicine and biology.* Sep 21 2012;57(18):5809-5821.

21. Dodd MS, Ball DR, Schroeder MA, et al. In vivo alterations in cardiac metabolism and function in the spontaneously hypertensive rat heart. *Cardiovascular research.* Jul 1 2012;95(1):69-76.

22. Reutter BW, Huesman RH, Brennan KM, Boutchko R, Hanrahan SM, Gullberg GT. Longitudinal Evaluation of Fatty Acid Metabolism in Normal and Spontaneously Hypertensive Rat Hearts with Dynamic MicroSPECT Imaging. *International journal of molecular imaging.* 2011;2011:893129.

23. Hajri T, Ibrahimi A, Coburn CT, et al. Defective fatty acid uptake in the spontaneously hypertensive rat is a primary determinant of altered glucose metabolism, hyperinsulinemia, and myocardial hypertrophy. *The Journal of biological chemistry.* Jun 29 2001;276(26):23661-23666.

24. Taegtmeyer H. Tracing cardiac metabolism in vivo: one substrate at a time. *Journal of nuclear medicine : official publication, Society of Nuclear Medicine.* May 1 2010;51 Suppl 1:80S-87S.

25. Iltis I, Kober F, Dalmasso C, Cozzone PJ, Bernard M. Noninvasive characterization of myocardial blood flow in diabetic, hypertensive, and diabetic-hypertensive rats using spin-labeling MRI. *Microcirculation.* Dec 2005;12(8):607-614.

26. Katz AM. *Physiology of the heart*. 5th ed. Philadelphia, PA: Wolters Kluwer Health/Lippincott Williams & Wilkins Health; 2011.

27. Denton RM, Randle PJ. Concentrations of glycerides and phospholipids in rat heart and gastrocnemius muscles. Effects of alloxan-diabetes and perfusion. *The Biochemical journal.* Aug 1967;104(2):416-422.

28. Korvald C, Elvenes OP, Myrmel T. Myocardial substrate metabolism influences left ventricular energetics in vivo. *American journal of physiology Heart and circulatory physiology.* Apr 2000;278(4):H1345-1351.

29. Remondino A, Rosenblatt-Velin N, Montessuit C, et al. Altered expression of proteins of metabolic regulation during remodeling of the left ventricle after myocardial infarction. *Journal of molecular and cellular cardiology.* Nov 2000;32(11):2025-2034.

30. Brooks WW, Shen SS, Conrad CH, Goldstein RH, Bing OH. Transition from compensated hypertrophy to systolic heart failure in the spontaneously

hypertensive rat: Structure, function, and transcript analysis. *Genomics.* Feb 2010;95(2):84-92.

31. Purushothaman S, Renuka Nair R, Harikrishnan VS, Fernandez AC. Temporal relation of cardiac hypertrophy, oxidative stress, and fatty acid metabolism in spontaneously hypertensive rat. *Molecular and cellular biochemistry.* May 2011;351(1-2):59-64.

32. Sharp TL, Dence CS, Engelbach JA, Herrero P, Gropler RJ, Welch MJ. Techniques necessary for multiple tracer quantitative small-animal imaging studies. *Nuclear medicine and biology.* Nov 2005;32(8):875-884.

33. Janabi M, Gullberg GT, O'Neil JP. Automated synthesis of [F-18]Fluorodihydrorotenol and [F-18]Fluoro-6-thia-heptadecanoic acid using GE's F_xF_N module. (To be submitted)

FIGURE CAPTIONS

Figure 1. (A) [^{18}F]FDHROL image of SHR showing substantial liver uptake; (B) [^{18}F]FTHA image of SHR again showing substantial liver uptake; (C) [^{18}F]FDG image showing relatively no liver uptake.

Figure 2. (A) Left-Ventricular Ejection Fraction (LVEF) showing significant ejection impairment for SHR starting at 20 months of age. (B) End-Diastolic Volume (EDV) showing dilated LV of SHR.
Note: numbers adjacent to the age labels correspond to samples measured for WKY and SHR respectively at the given age. This notation is consistent throughout the remaining figures.

Figure 3. Glucose (A) and free fatty acid (B) circulating plasma concentrations as a function of age.

Figure 4. (A) [^{18}F]FDG influx constant and (B) [^{18}F]FTHA influx constant in myocardium as a function of age.

Figure 5. Comparison of [^{18}F]FDG time activity curves for left-ventricular blood pool (A) and myocardial tissue (B) in SHR and control model at ~8 months of age.

Figure 6. Example of closed-form fitting algorithm implemented on 14-month old SHR imaged using [^{18}F]FDHROL.

Figure 7. [^{18}F]FDHROL wash-in rate constant (K_1).

Figure 1

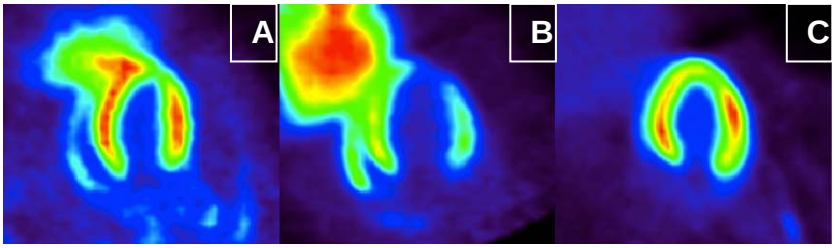

Figure 2

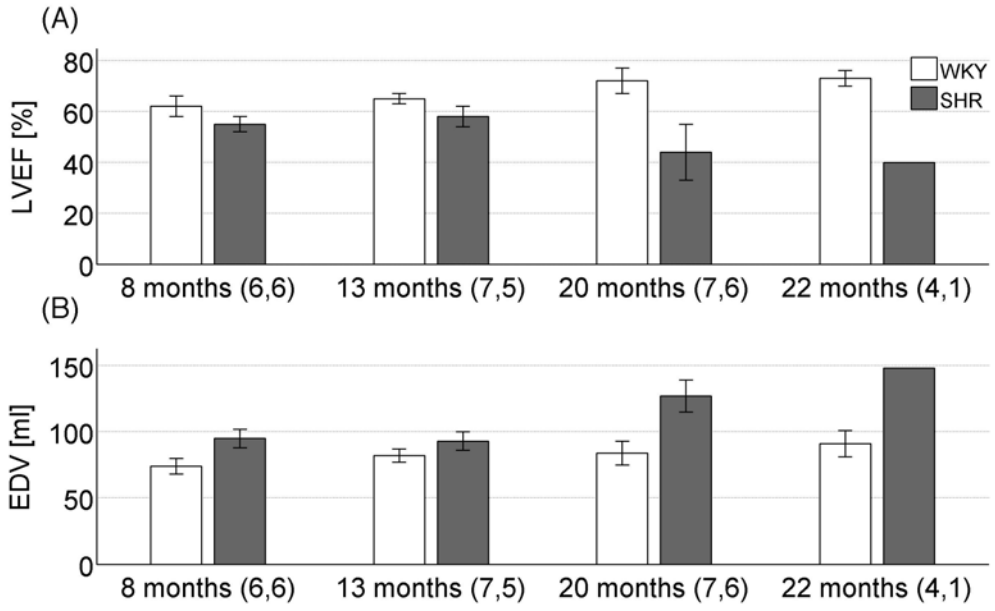
(A)
LVEF [%]
80
60
40
20
0
WKY
SHR
8 months (6,6)
13 months (7,5)
20 months (7,6)
22 months (4,1)
(B)
EDV [ml]
150
100
50
0
8 months (6,6)
13 months (7,5)
20 months (7,6)
22 months (4,1)

Figure 3

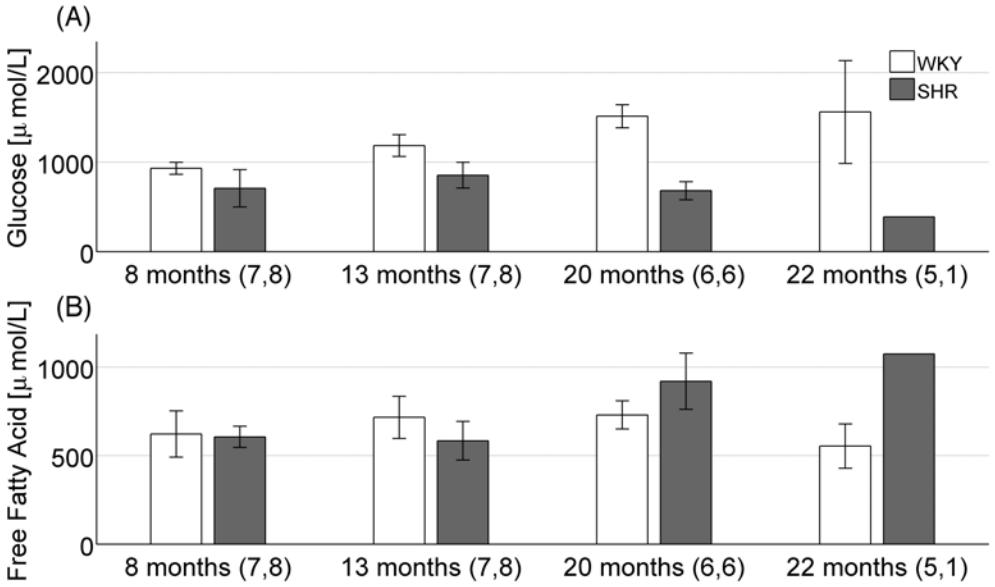
(A)
Glucose [µ mol/L]
2000
1000
0
WKY
SHR
8 months (7,8)
13 months (7,8)
20 months (6,6)
22 months (5,1)
(B)
Free Fatty Acid [µ mol/L]
1000
500
0
8 months (7,8)
13 months (7,8)
20 months (6,6)
22 months (5,1)

Figure 4

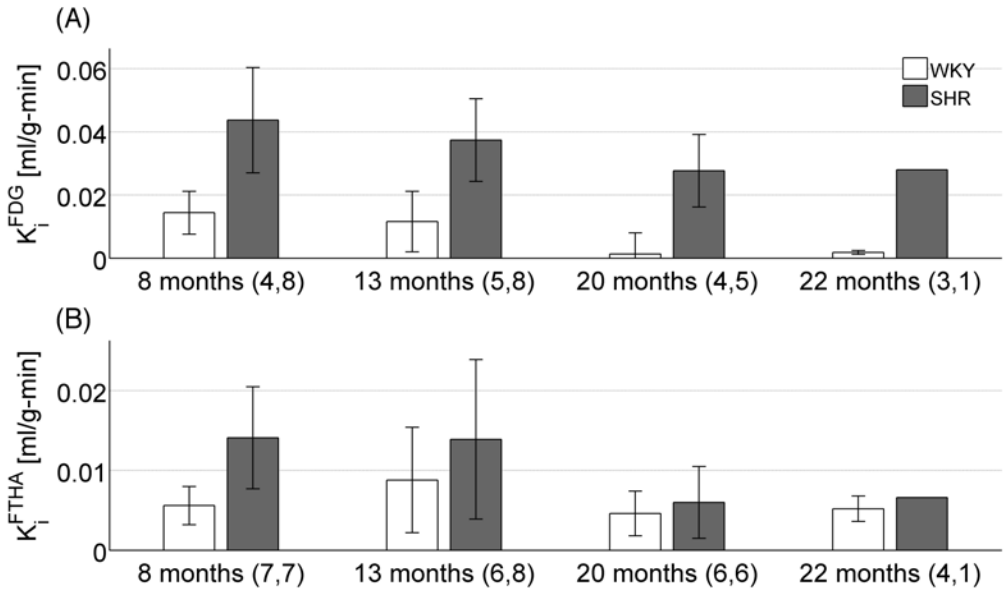
(A)
WKY
SHR
K_i^{FDG} [ml/g-min]
0.06
0.04
0.02
0
8 months (4,8)
13 months (5,8)
20 months (4,5)
22 months (3,1)
(B)
K_i^{FTHA} [ml/g-min]
0.02
0.01
0
8 months (7,7)
13 months (6,8)
20 months (6,6)
22 months (4,1)

Figure 5

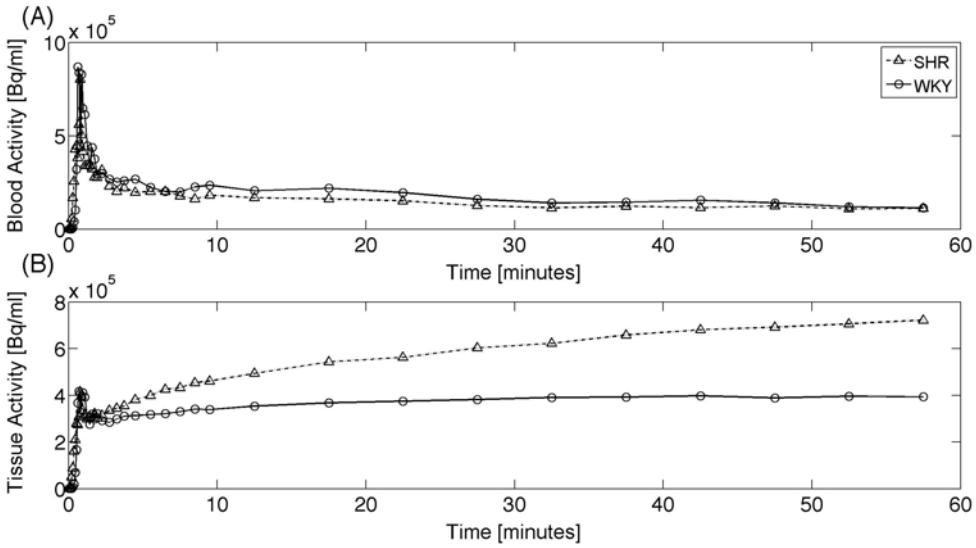
(A)
x 10^5
Blood Activity [Bq/ml]
SHR
WKY
Time [minutes]
(B)
x 10^5
Tissue Activity [Bq/ml]
Time [minutes]

Figure 6

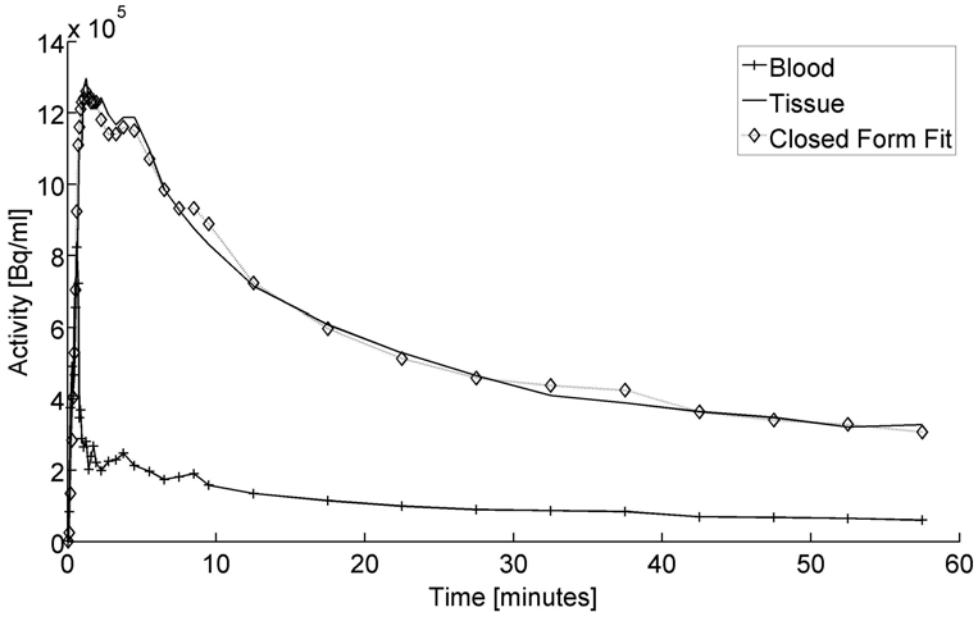
x 10^5
14
12
10
8
6
4
2
0
Activity [Bq/ml]
0
10
20
30
40
50
60
Time [minutes]
Blood
Tissue
Closed Form Fit

Figure 7

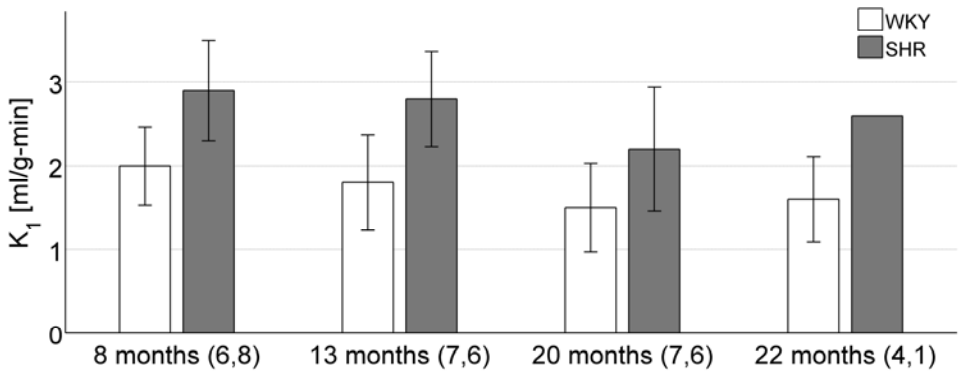
WKY
SHR
K_1 [ml/g-min]
0
1
2
3
8 months (6,8)
13 months (7,6)
20 months (7,6)
22 months (4,1)